Geol Rundsch (1993) 82: 121–135

G. Jarrar · H. Wachendorf · D. Zachmann

A Pan-African alkaline pluton intruding the Saramuj Conglomerate, south-west Jordan

Received: 15 August 1990 / Accepted: 3 February 1993

Abstract The geological setting, petrography and bulk mineral chemistry of a monzodiorite and a presumably consanguineous megaporphyry with large (up to 25 cm) labradorite megacrysts, both intruding the upper Proterozoic Saramuj Conglomerate in south-west Jordan (south eastern shore of the Dead Sea), were examined. The crystallization temperatures of the monzodiorite and the megaporphyry as determined from pyroxene thermometry and supported by contact metamorphic mineralogy are about 700 and 900 °C, respectively. The intrusion depth of the monzodiorite is about 3–4 km. The monzodiorite was emplaced in the Saramuj Conglomerate at about 595 ± 2 Ma ago according to Rb/Sr and U/Pb age determinations.

The stratigraphic positions of the monzodiorite, megaporphyry and their host rock (the Saramuj Conglomerate) were compared with time-equivalent lithologies in the Arabian–Nubian Shield.

Key words Pan-African Orogeny – alkaline plutons – south-west Jordan – thermometry – age determinations

Introduction

The evolution of the Pan-African Orogeny was terminated with the formation of a rift-related magmato-sedimentary intramontane molasse. This magmatism is of alkaline character and displays closely related plutonic and volcanic features. A dolerite porphyry in Jordan with microscopically unzoned labradorite megacrysts, referred to herein as a megaporphyry, represents a conduit filling and is presumably consanguineous with an epizonal monzodiorite stock. The monzodiorite was mapped by Bender (1974) as a diorite overlain by the Saramuj Conglomerate with a profound erosional unconformity. On the basis of field and petrographic criteria we reinterpret the monzodiorite and the megaporphyry to intrude the Saramuj Conglomerate. The megaporphyry is described here for the first time.

Lenz et al. (1972) obtained 594 ± 8 and 585 ± 8 Ma by K/Ar dating of biotites from the monzodiorite. Brook et al. (1990) described the monzodiorite as intensely weathered and not suitable for isotopic dating. This alteration explains their imprecise results (Rb/Sr whole rock age 490 ± 210 Ma).

The purpose of this paper is to report the petrography, bulk and mineral chemistry of a monzodiorite and a related megaporphyry and to constrain the age of the Saramuj Conglomerate to compare this magmato-sedimentary sequence with time-equivalent molasse sequences of the Arabian–Nubian Shield.

Ghaleb Jarrar
Department of Geology, University of Jordan, Amman, Hashemite Kingdom of Jordan

Horst Wachendorf · Dieter Zachmann
Institut für Geowissenschaften, Pockelsstraße 4, Technische Universität Braunschweig, 3300 Braunschweig, Germany

Correspondence to: H. Wachendorf

Geological setting and field aspects

The studied area is part of the northernmost exposure of the late Proterozoic basement along the Wadi Araba-Dead Sea Rift (Fig. 1). The basement consist mainly of granitoids and sporadic occurrences of mafic and metamorphic rocks. The final stage of the Pan-African evolution is marked by the post-orogenic deposition of molasse sediments and a bimodal magmatic activity. The molasse sediments are typified by the Saramuj Conglomerate (Blanckenhorn, 1912). In addition to the Saramuj Conglomerate, which has a minimum exposed thickness of 200 m in its type locality (Jarrar et al., 1991), the molasse encompasses a slate–pyroclastic succession about 250 m thick. This was mapped by Bender (1974) as the Slate–Greywacke Series and later renamed as the Hiayala Volcanoclastic Formation (McCourt, 1988). The Saramuj Conglomerate, which consists principally of granitic components, was intruded by a monzodioritic

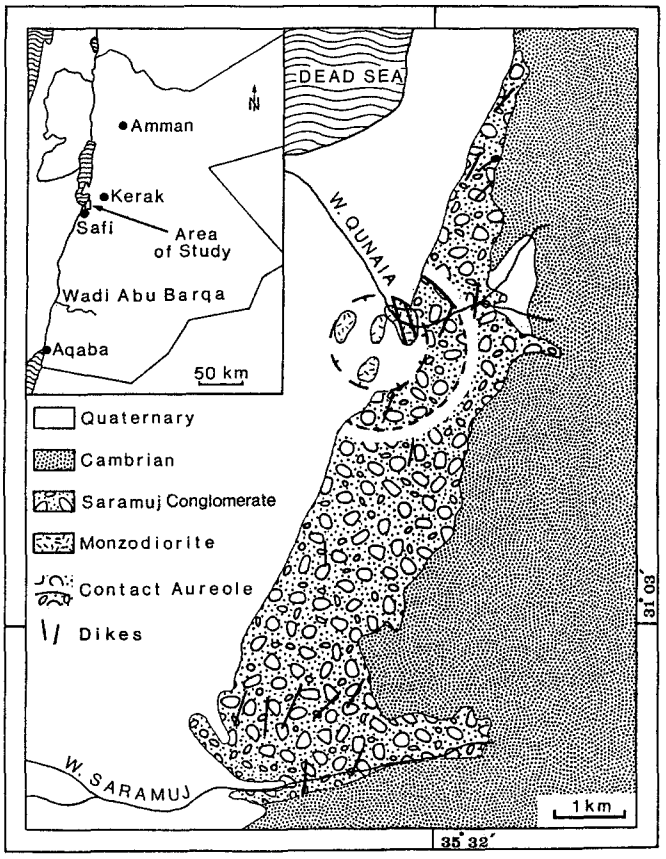

Fig. 1. Location map of the study area

stock. The monzodiorite and the Saramuj Conglomerate were again intruded by several dykes and cut by a conduit filled with a megaporphyry. The megaporphyry and the monzodiorite are largely covered by recent alluvial fans.

Isotopic data document the evolution of the basement from 800 to 600 Ma (Lenz et al., 1972; Jarrar, 1985; Brook et al., 1990). Calc-alkaline granitoids were mainly emplaced between 625 and 600 Ma. The crystalline basement is separated by an intra-Proterozoic unconformity from the molasse sequence. This regional unconformity is mainly exposed in the area of Wadi Abu-Barqa (Figure 1) and hidden in the type locality of the Saramuj Conglomerate, i.e. Wadi Saramuj.

The molasse sediments are intruded by a monzodioritic stock, producing a contact metamorphic aureole. This finding contradicts the interpretation of Lenz et al. (1972). These workers placed the monzodiorite in the 'older intrusive rocks', i.e. the pre-molasse sequence. The contact aureole around the monzodiorite has a width of up to 1 km in the Saramuj Conglomerate and proves the intrusive relationship between the monzodiorite and the Saramuj Conglomerate. The thermally metamorphosed Saramuj Conglomerate is dark coloured and very hard in contrast with the green coloured epimetamorphosed Saramuj Conglomerate. The dark colour is due to the abundance of biotite and other ferromagnesian minerals.

The coarse grained, grey coloured and occasionally deeply weathered monzodiorite is exposed along the WNW-trending, steep-sided Wadi Qunaia forming four separated outcrops within an area of 1 square kilometer. The restricted exposures of the megaporphyry hinder an exact reconstruction of the original shape of the magmatic complex. The megaporphyry forms dykes with a thickness of up to 5 m which can be followed for several tens of metres along a WNW to north-west strike direction. These dykes are displaced by Tertiary to subrecent WNW and NNE trending rift-related faults.

The megaporphyry is characterized by the presence of giant, up to 25 cm (average 10 cm) large unzoned labradorite phenocrysts (Fig. 2a) and monzodioritic xenoliths, up to 1 m in diameter, which are set in a fine grained, greenish grey groundmass (Fig. 2c). The greenish white megacrysts range between 28 and 42% with an average of 34% by volume of the megaporphyry. These megacrysts are dominantly oriented at random, which together with the xenoliths exclude a laminar magmatic flow process. Additionally, the large xenoliths indicate a relatively rapid transport to a subsurface level by a highly fluid-charged magma. An orientation of the megacrysts along flow lines is displayed only subordinately and is presumably restricted to the margins of the feeder channels (Fig. 2b). The labradorite phenocrysts are predominantly megacrystic, although distinctly small crystals are also common. Moreover, the labradorite phenocrysts display a glomeroporphyritic texture (Fig. 2d).

The presence of a bimodal rather than a seriate distribution of phenocrysts also favours a rapid magmatic ascent (Cox et al., 1979). In contrast with the megacrysts from anorthositic complexes (e.g. Phinney et al., 1988), the plagioclases of the megaporphyry exhibit both equidimensional and lathy to platy habits, which signifies poor sorting due to a more turbulent transport to the surface.

The monzodiorite contains xenoliths of variable composition (e.g. plutonic and volcanic pebbles from the Saramuj Conglomerate). Most of these xenoliths are distributed in the vicinity of the contact with the Saramuj Conglomerate. In addition, a 1 m syenite xenolith was also recorded.

Petrography

The monzodiorite is a coarse grained, equigranular, grey coloured rock and consists of plagioclase, interstitial alkali feldspar, diopside, olivine, biotite and accessories of Fe and Ti oxides and apatite. The plagioclase occurs as platy, subhedral crystals with a size range of 5–15 mm, which are characterized by prominent albite and Karlsbad twinning. Pericline twinning is less common. The plagioclase content is about 65% of the rock by volume. Diopside (10%) is subhedral to euhedral and ranges in size from 0.5 to 0.15 mm. It is often included in the other minerals (e.g. biotite, alkali feldspar and less commonly in plagioclase). The pyroxene has a pale brown colour and is slightly pleochroic. Olivine occurs in colorless, sub- to euhedral cracked grains. It has an average grain size of 0.8 mm. Small grains are also often included in the

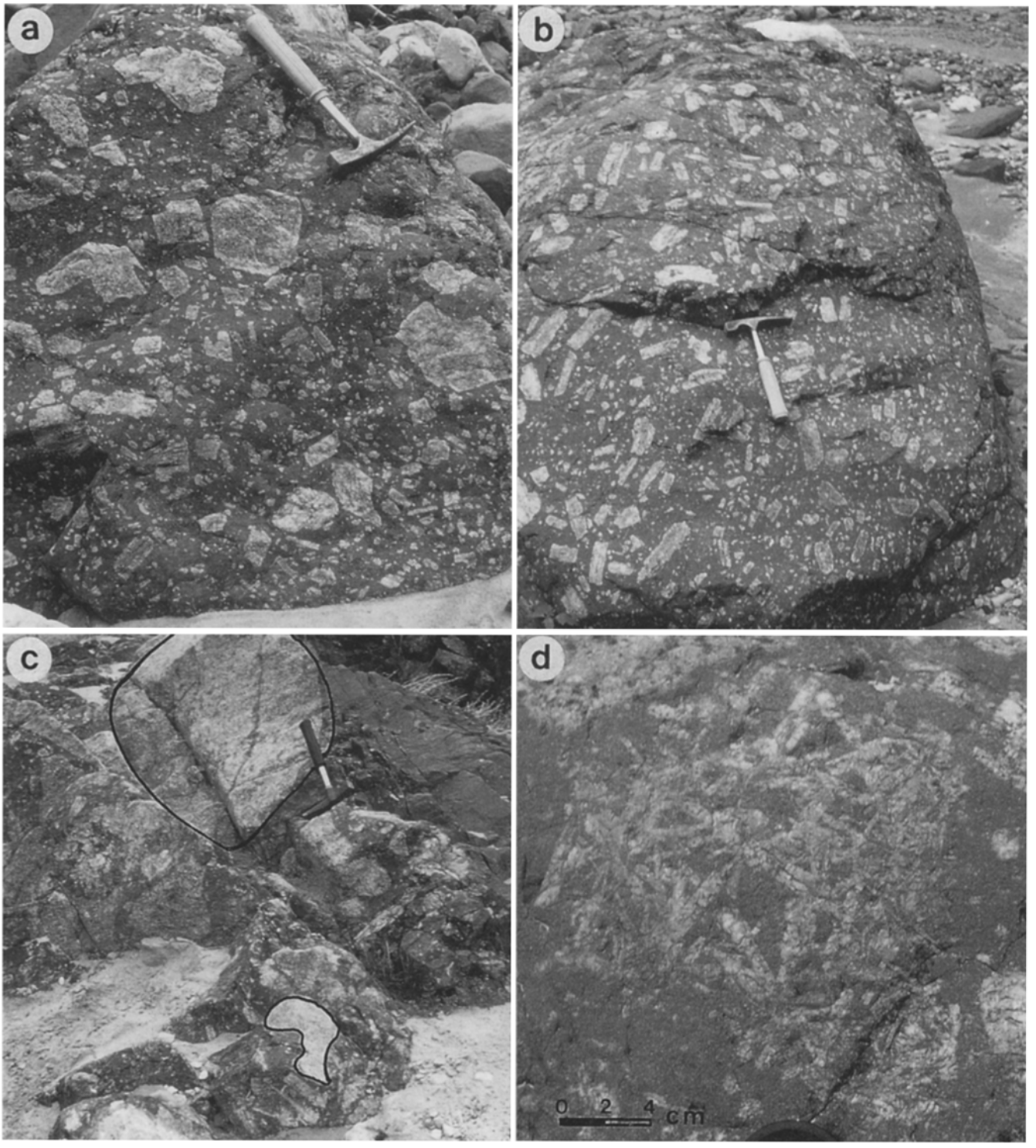

Fig. 2. a Megaporphyry with random orientation and bimodal size distribution of plagioclase megacrysts. b Megaporphyry with fluidal orientation of the plagioclase megacrysts. c Monzodioritic xenoliths in the megaporphyry. d Glomeroporphyritic texture in the megaporphyry

pyroxene. The olivine is partially to totally altered to light green serpentine and/or deep red iddingsite along cracks. It accounts for 8% of the rock.

Alkali feldspar (12–15%) is present in the form of about 2 mm anhedral, interstitial grains. It is typically cryptoperthitic. The biotite (8%) is subhedral, strongly pleochroic and forms melanocratic aggregates with the oxides, diopside and olivine (Fig. 3a). Large poikilitic crystals enclosing diopside, olivine, oxides and apatite are common. Euhedral apatite and eu- to subhedral opaques are present in clusters in the other minerals and account for 6% of the rock by volume.

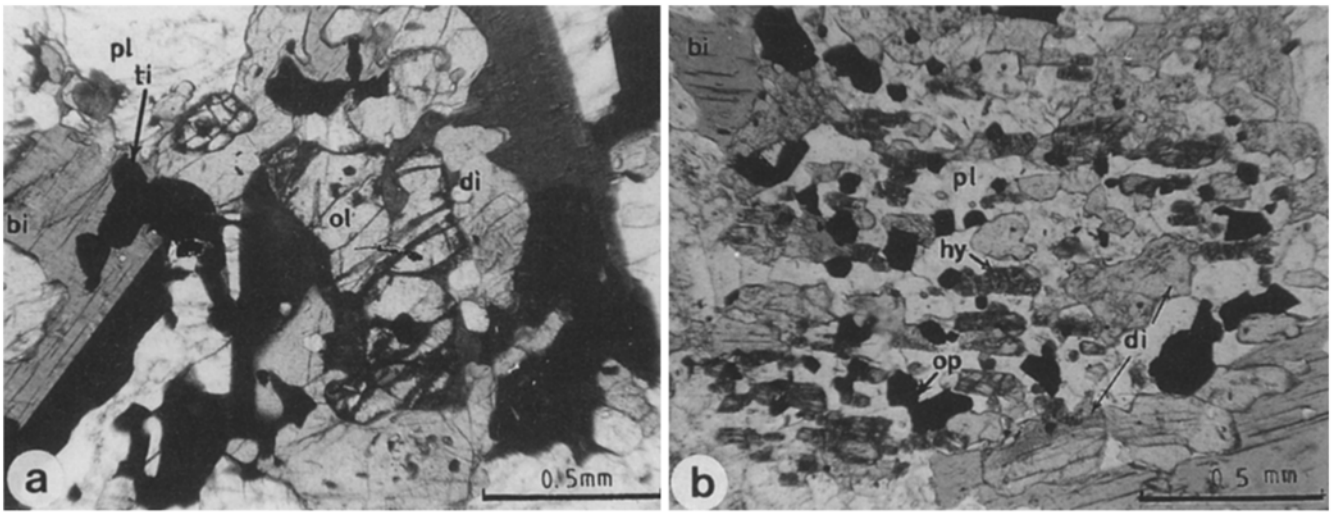

Fig. 3. a Aggregate of melanocratic minerals in the monzodiorite. Olivine grains are mostly included in the diopside. b Hypersthene – diopside – biotite – plagioclase hornfels from the innermost aureole. Symbols: bi = biotite; di = diopside; hy = hypersthene; pl = plagioclase; ol = olivine; op = opaques and ti = titanomagnetite

The modal analysis corresponds to a monzodiorite/gabbro. However, the average composition of the plagioclase is An_{49} (Table 6). We therefore consider the rock to be a monzodiorite rather than a monzogabbro following the recommendations of the IUGS (Streckeisen, 1976), although the olivine content is unusually high for a diorite.

Textural relationships in the monzodiorite suggest the sequence of magmatic crystallization presented in Figure 4.

The megaporphyry is composed of unzoned, polysynthetically twinned labradorite megacrysts which are set in a fine grained groundmass of plagioclase and pyroxene. Corrosion embayments in the plagioclase megacrysts are common. Occasionally the groundmass is intruded along twinning planes. The megacrysts are partly sericitized, which is reflected in the high potassium content of the megacrysts. The plagioclases of the groundmass (65% of the groundmass by volume) are up to 0.5 mm long and less than 0.1 mm wide. They are highly sericitized, subhedral and form together with large anhedral Ti augite (about 30% of the groundmass by volume) a typical ophitic texture. Microprobe analyses of the groundmass plagioclase yield anorthite contents between 1 and 39%. This extreme variation in the An content is probably due to late magmatic albitization of the plagioclase. Taking the bulk chemical composition of the groundmass into account the analysis of sample F3/2 (Table 6) with An_{24} can be considered as representative. Opaques are titanomagnetite and constitute together with apatite and zircon, about 5% of the groundmass.

The monzodiorite developed a contact metamorphic aureole, the width of which is about 1 km. The groundmass of the Saramuj Conglomerate is completely recrystallized to a hornfels and developed the following two mineral parageneses: (1) hornblende + diopside + hypersthene + biotite + plagioclase + quartz + opaques (Fig. 3 b); and (2) biotite + plagioclase + quartz + opaques.

The first paragenesis is diagnostic for the innermost aureole. The two varieties lack a preferred orientation and are characterized by the presence of poikiloblastic textures. On the other hand, the epimetamorphosed groundmass consists to a large extent of quartz and feldspar as well as rock fragments and considerable amounts of chlorite and epidote. The latter two minerals

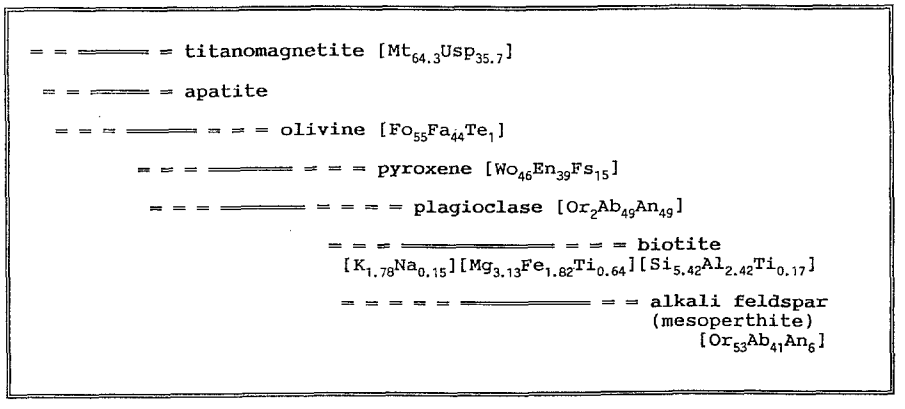

Fig. 4. Schematic representation of the crystallization sequence of the monzodiorite as deduced from the petrography

are widespread in the greenschist facies for which a minimum temperature of 250 °C can be assumed (e.g. Frey et al., 1991). A geothermal gradient of at least 75 °C km^{-1} for the Pan-African crust (Reymer et al., 1984) implies a minimum burial of the Saramuj Conglomerate between 3 and 4 km.

Typical contact metamorphic minerals, i.e. andalusite and cordierite have not been recorded in 15 thin sections investigated from the innermost aureole. This can be attributed to the lack of an appropriate chemistry (average Al_2O_3 in the Saramuj Conglomerate = 14 wt.%; Jarrar et al., 1991).

Isotopic age data

The isotopic analyses were performed at the Zentrallaboratorium für Geochronologie (ZLG) at the University of Münster, Germany. The chemical procedure for the zircon analysis applies the method as outlined by Krogh (1973) and is described in detail by Jarrar (1985). For the common lead correction an isotopic composition according to the model of Stacey and Kramers (1975) was assumed. The assigned analytical errors are 1% for $^{207}Pb/^{235}U$ and $^{206}Pb/^{238}U$ and 0.5% for $^{207}Pb/^{206}Pb$.

Rb/Sr analyses were carried out according to the method described by Blaxland et al. (1979). The analytical errors are assigned on the basis of replicate analyses at 1.5 and 0.05% for the $^{87}Rb/^{86}Sr$ and $^{87}Sr/^{86}Sr$ ratios, respectively. The mass spectrometric measurements of U, Pb, Rb and Sr were carried out on a Teledyne 12 inch 90° solid source mass spectrometer. The decay constants used for the calculations are those recommended by Steiger and Jäger (1977).

The results of Rb/Sr and U/Pb age determinations are presented in Table 1. A biotite whole rock age of 596 ± 6 Ma and $^{87}Sr/^{86}Sr$ initial ratio of 0.703 64 ± 0.000 13 have been calculated. For the calculation of the discordia the York (1969) and Ludwig (1980) programs were used.

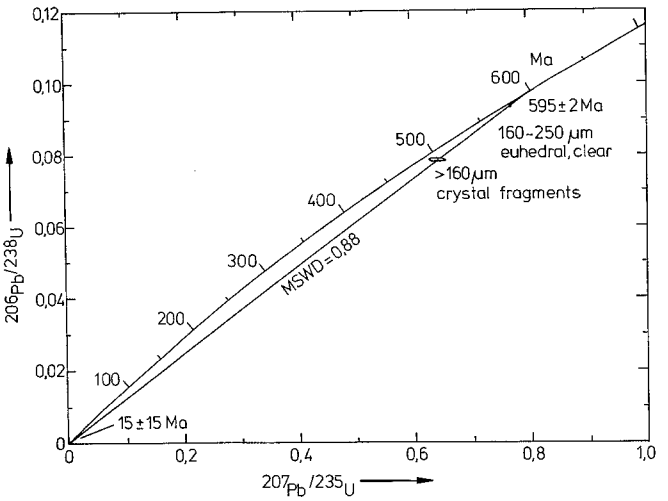

Fig. 5. Discordia diagram of two zircon populations from the monzodiorite

Only two zircon populations were obtained from an about 50 kg sample. These two populations were analysed and produced discordant points which define an upper intercept of 598 ± 3 Ma and a lower intercept of 111 ± 17 Ma. The upper intercept can be taken as the crystallization age of the zircons whereas the lower intercept is geologically meaningless.

An alternative interpretation of the data is based on the assumption that an episodic loss of lead was induced by Tertiary uplift in connection with Red Sea rifting, i.e. the lower intercept passes through 15 Ma. Cooper et al. (1979) and Pallister et al. (1988) applied this model to zircon data from a large area of the Arabian Shield. This model is consistent with the Phanerozoic evolution of the Arabian Shield, which acted as a stable platform between the end of the Proterozoic and Tertiary rifting. Applying

Table 1. Radiometric data of the monzodiorite

Rb/Sr data

Sample	Rb (ppm)	Sr (ppm)	$^{87}Rb/^{86}Sr$	$^{87}Sr/^{86}Sr$	Age and initial ratio
JB7 (WR)	116	1046	0.3230 ± 22	0.70639 ± 6	596 ± 6 Ma
JB7 (biotite)	831	33	76.495 ± 136	1.35377 ± 12	(Sr_i 0.70364 ± 0.00013)

U/Pb data of two zircon populations from a monzodiorite sample (50 kg)

Size	Description	U (ppm)	Pb (ppm)	Measured ratios			Calculated ratios		
				208/206	207/206	206/204	206/238	207/235	207/206
>160 µm	euhedral and clear	1294	168	0.54662	0.06269	4560.7	0.09355	0.77076	0.05976
160 to 250 µm	skeletal and brown	486	53	0.55777	0.06376	3224.3	0.07855	0.64173	0.05926

	Apparent ages (Ma)		
	206/238	207/235	207/206
>160 µm	576.5	580.2	594.8
160–250 µm	487.4	503.4	576.5

the above model to the monzodiorite zircons, we obtain an upper intercept at 595 ± 2 Ma and a lower intercept at 15 ± 15 Ma (Fig. 5). The upper intercept coincides with the $^{207}Pb/^{206}Pb$ age of the more concordant data point, i.e. 594.8 Ma. Therefore we prefer to consider an age of 595 ± 2 Ma as the emplacement age of the monzodiorite.

To recapitulate, the age of 595 Ma obtained from both U/Pb and Rb/Sr biotite whole rock techniques can be taken as the intrusive age of the monzodiorite. However, the slightly younger age of Lenz et al. (1972) can be attributed to a loss of radiogenic argon.

Geochemistry

Bulk chemistry

Inductively coupled plasma atomic emission spectrometry (ICP-AES) and X-ray fluorescence techniques were applied for the bulk chemical analyses of seven monzodiorite samples, two groundmass samples and three plagioclase megacrysts of the megaporphyry. The groundmass and the microprobe megacryst analyses were

Table 2. Major (wt.%) and trace (ppm) element contents, element ratios and CIPW norms of the monzodiorite and the megaporphyry

	Monzodiorite							Megaporphyry		
	JB7	49**	51**	53**	CI2	CII2	C43	C44	GJ	4
SiO_2	50.19	49.90	49.16	53.17	57.51	53.68	52.82	48.30	50.16	50.71
TiO_2	1.17	1.38	1.27	0.93	0.80	1.00	0.78	2.09	2.49	1.55
Al_2O_3	17.80	17.73	19.07	20.50	16.25	20.03	21.55	15.50	16.07	20.01
Fe_2O_3	2.67	2.88	2.77	2.43	2.30	2.50	2.28	3.59	3.99	3.05
FeO	5.52	6.07	5.61	3.73	4.25	3.85	3.87	9.07	6.44	4.81
MnO	0.14	0.22	0.24	0.12	0.09	0.12	0.10	0.15	0.18	0.12
CaO	7.14	6.19	6.87	5.86	2.87	5.67	8.40	6.72	5.40	7.74
MgO	4.25	3.78	3.38	2.33	3.55	2.57	2.42	4.42	4.30	2.88
Na_2O	4.19	4.04	3.74	4.42	5.68	4.05	3.36	3.83	4.10	4.13
K_2O	2.99	3.82	4.03	3.93	2.98	3.52	1.46	1.36	1.91	1.23
P_2O_5	0.79	0.96	1.08	0.69	0.70	0.60	0.50	0.79	0.71	0.50
LOI	1.38	1.86	1.82	1.28	2.60	1.61	0.87	3.28	2.78	1.88
Total	98.22	98.83	99.05	99.40	99.58	99.20	98.41	99.10	98.53	98.61
Y	24	25	31	22	26	28	21	37	26	22
Zr	184	152	207	144	167	88	49	167	186	119
Ga	21	20	21	18	–	–	–	–	–	–
Nb	13	9	11	7	18	18	14	24	33	21
Sc	17	–	–	–	18	19	9	27	18	15
V	172	–	–	–	184	152	191	291	226	175
Cr	53	–	–	–	93	65	46	47	38	32
Ba	1354	1570	1337	2200	1128	1113	979	984	1419	892
Ni	24	–	–	–	48	32	41	92	83	63
Cu	97	–	–	–	96	98	224	64	185	85
Zn	80	–	–	–	134	112	118	144	114	91
Yb	2.8	3	3	2	4.1	2.7	3.7	4.9	4.1	3.2
Co	46	–	–	–	53	44	53	88	64	53
Sr	1033	1075	1106	1602	862	763	1673	1015	1011	1125
Rb	117	117	154	106	–	–	–	–	–	–
$Na_2O + K_2O$	7.18	7.87	7.78	8.35	8.66	7.57	4.82	5.19	6.01	5.36
Mg #	0.58	0.53	0.52	0.53	0.60	0.54	0.53	0.47	0.54	0.52
K/Rb	214	274	220	311	–	–	–	–	–	–
K/Ba	18.49	20.43	25.30	15.00	22.16	26.52	12.51	11.59	11.29	–
q	–	–	–	–	2.48	0.75	5.75	–	1.42	0.59
or	18.65	23.28	24.50	23.67	17.97	21.32	8.85	8.48	11.79	7.55
ab	27.32	29.45	25.22	36.50	49.06	35.12	29.15	34.18	36.23	36.32
an	22.09	19.55	24.01	24.96	9.87	24.81	39.38	22.24	20.68	33.70
ne	5.47	3.14	3.97	0.88	–	–	–	–	–	–
c	–	–	–	–	0.70	0.38	–	–	–	–
di	8.01	4.63	3.11	0.06	–	–	–	–	1.98	5.04
hy	–	–	–	–	13.87	10.23	10.40	10.84	15.20	9.15
ol	10.09	10.64	10.00	6.91	–	–	–	6.47	–	–
mt	4.09	4.31	4.13	3.59	3.40	3.71	3.39	5.49	6.04	4.60
il	2.35	2.70	2.48	1.80	1.55	1.95	1.52	4.19	4.94	3.06
ap	1.98	2.35	2.63	1.67	1.69	1.46	1.21	1.97	1.76	–
DI	51.44	55.87	53.69	61.05	69.51	57.18	43.75	42.66	49.44	44.46

Mg # = at. ratio ($Mg/Mg + Fe^{2+}$); DI = differentiation index; ** samples from McCourt (1988); C44 and GJ are groundmass analyses of the megaporphyry; 4 = average chemical composition of the megaporphyry using the phenocryst : groundmass ratio of 34 : 66. The CIPW norms were calculated assuming $Fe_2O_3 = TiO_2 + 1.5$ (Irvine and Baragar, 1971).

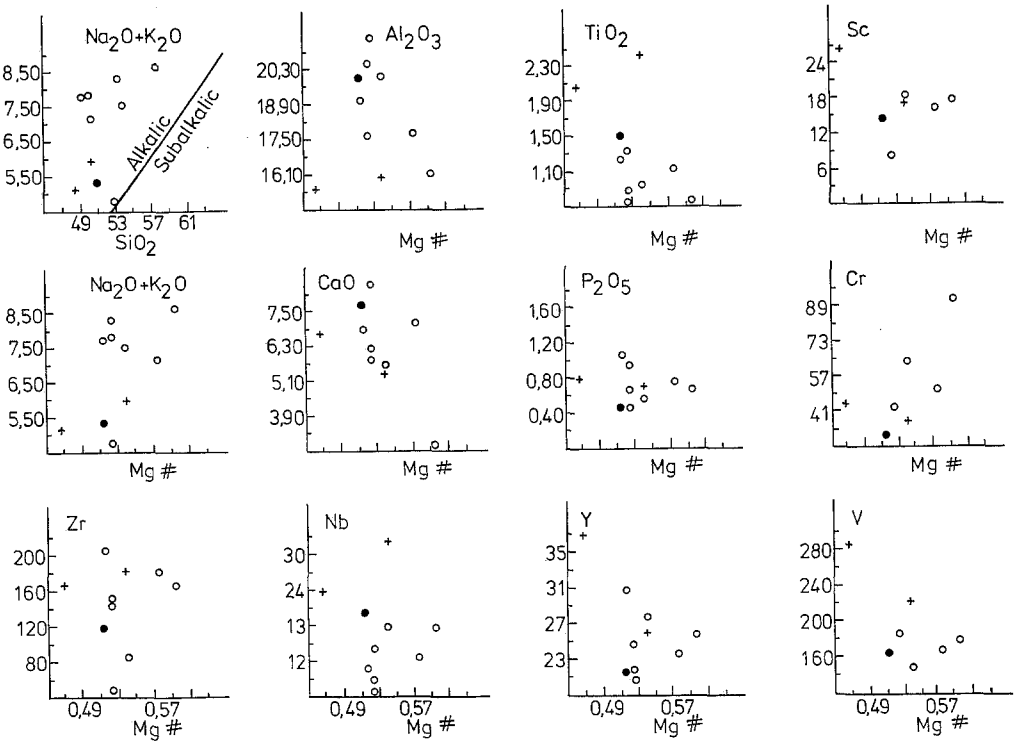

Fig. 6. Silica alkali diagram and Mg # versus Al_2O_3, TiO_2, total alkalies, CaO, P_2O_5, Sc, Cr, Zr, Nb, Y and V. Symbols: open circles = monzodiorite; closed circles = average megaporphyry; pluses = groundmass of the megaporphyry; Mg # = atomic ratio (MgO/MgO + FeO). The divider in the alkali silica diagram is after Miyashiro (1978)

used to calculate the average chemistry of the megaporphyry (Table 2, analysis 4) by taking the megacryst/groundmass ratio of 34:66. This ratio was deduced from the determination of the area distribution of the megacrysts and groundmass on three representative field photographs. Three of the monzodiorite analyses were taken from McCourt (1988). The major and trace element concentrations and the CIPW norms are listed in Table 2.

Four monzodiorite samples are nepheline normative whereas the other three and the megaporphyry are quartz normative. Neither nepheline nor quartz were recorded in the thin sections. In the alkali silica diagram (Fig. 6) the monzodiorite and the megaporphyry plot in the alkaline field. The alkaline character of both rock types suggests a rift-related anorogenic environment which is in accordance with the geological setting of the intermontane molasse sequence. The atomic $Mg/Mg + Fe^{2+}$ ratios (Mg #) of the monzodiorite ranges between 0.52 and 0.60 and averages 0.55 whereas the megaporphyry has a value of 0.52.

Major and trace elements are plotted against the Mg # of both rock types (Fig. 6). Inspection of Fig. 6 reveals that the monzodiorite is enriched in Zr, Y, V, Cr, P_2O_5, Sc, Ba, Sr and total alkalies and depleted in Al_2O_3, TiO_2, CaO and Nb relative to the megaporphyry. Moreover, the monzodiorite shows decreasing concentrations of Al_2O_3, CaO, P_2O_5 and TiO_2 with increasing Mg #. On the other hand, Sc, Cr, V, Nb, Y, Zr and total alkalies display an increasing trend. It is noteworthy that the apparent scatter of the data points is due to the small number of bulk analyses.

Selected trace and minor elements of the monzodiorite and the megaporphyry are normalized to chondrite compositions (Thompson et al., 1984). Both rock varieties exhibit more or less similar patterns of enrichment and depletion (Fig. 7), which supports a common origin. The following elements are enriched in decreasing order: Ba > Rb > K > Sr > P > Nb > Zr > Ti > Y > Yb. The large ion lithophile elements (LILE) (e.g. Rb, Ba, K) are highly enriched in both rock types relative to the high field strength cations (P, Zr, Y, Ti). However, the enrichment is generally more pronounced in the monzodiorite despite the higher Mg #. Therefore, as an additional source for the enrichment of the monzodiorite in the LILE the assimilation of crustal material is supposed. The LILE chondrite normalized patterns (Fig. 7) of the studied rocks are comparable with those of the rift zone magmatism (Wilson, 1989) with the exception of a Nb depletion.

Fig. 7. Spider diagram of incompatible element abundances normalized to chondrite values (Thompson et al., 1984). Symbols: open circles = average monzodiorite; closed circles = average megaporphyry

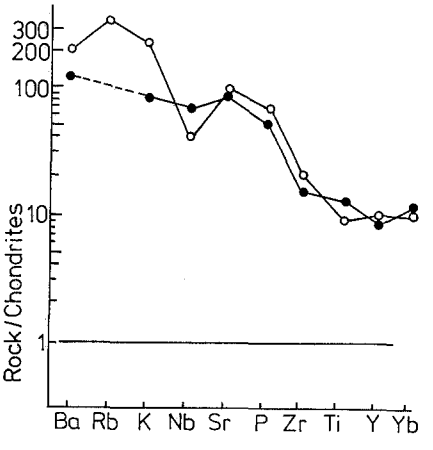

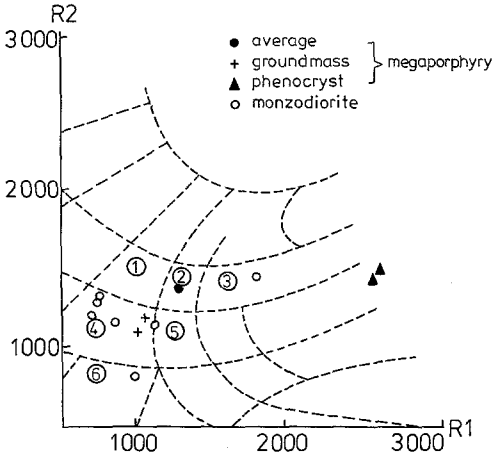

Fig. 8. R1 – R2 (De La Roche et al., 1980) diagram. 1 = syenogabbro; 2 = monzogabbro; 3 = gabbro/diorite; 4 = syenodiorite; 5 = monzonite and 6 = syenite. R1 = 4Si – 11(Na + K) – 2(Fe + Ti); R2 = 6Ca + 2Mg + Al

The Nb depletion is also displayed by the spider diagram (Fig. 7). A more pronounced negative Nb anomaly is typical of calc-alkaline basalts. Nevertheless, such an anomaly can also be developed in contamined within-plate basalts (Wilson, 1989).

Friz-Töpfer (1991) discussed the geochemistry of late Pan-African dyke swarms from Wadi Feiran, southern Sinai. Although the three dyke swarms were emplaced in an extensional tectonic setting, two generations (S1 and L1) display subduction-related features (e.g. Nb – Ta negative anomalies). Friz-Töpfer related the oldest generation (S1, age 591 ± 9; Stern and Manton, 1987) to calc-alkaline rocks from an active continental margin. On the other hand, the second generation (L1) indicates an increasing contribution of continental components to the melt chemistry. Friz-Töpfer (1991) concluded that the chemical differences encountered by the studied dyke swarms reflect differences in the chemistry of the source and are not linked to a changing tectonism.

Fitton et al. (1988) reported a strong negative Nb anomaly for late Cenozoic basalts from the western USA, although these basalts were clearly erupted in an extensional tectonic setting 20 Ma after the termination of the subduction along the Pacific. They suggested that the Nb depletion was inherited from the subcontinental lithospheric mantle which became metasomatized above the subduction zone.

In contrast with the LILE enrichment, the compatible elements (e.g. Cr and Ni) are strongly depleted. The averages of Cr and Ni of the monzodiorite are 64 and 36 ppm, respectively. The corresponding values of the megaporphyry are 39 and 79 ppm (Table 2).

On the R1 – R2 diagram of De La Roche et al. (1980) the monzodiorite and megaporphyry occupy the fields of gabbro, monzogabbro, gabbro/diorite, syenite and syenodiorite, with the latter being mostly represented (Figure 8). The average syenodioritic character of the monzodiorite is caused by the high total alkalies (7.18 – 8.66 wt.%). The high alkali content is also reflected in the appearance of relatively high orthoclase (up to 25%) and nepheline (up to 5.5%) in the CIPW norms. The presence of high contents of modal biotite explains the inconsistency between normative (CIPW) and modal mineralogy. The possible assimilation of crustal material is inferred from syenite xenoliths and some pebbles from the Saramuj Conglomerate, which could have resulted in the shift of the data points to the field of syenodiorite. No exposure of syenite in the vicinity of the studied rocks has been recorded.

Mineral chemistry

All mineral analyses were performed on polished thin sections utilizing a CAMECA electron microprobe at the Mineralogical Institute/Kiel University, Germany. The accelerating voltage and beam current were 15 kV and 15 nA, respectively.

Opaques. The chemical analyses of two opaque grains from the monzodiorite are given in Table 3. Endmember compositions were calculated by applying the procedure of Carmichael (1967). The composition of the opaques corresponds to titanomagnetite ($Mt_{64.33}Usp_{35.67}$). Unfortunately, titanomagnetite without ilmenite cannot be used to estimate the temperature of crystallization.

Olivine. Analyses and structural formulae of seven olivine grains from the monzodiorite are listed in Table 4. The composition of these olivines varies from Fo_{52} to Fo_{55}. There is a gradual increase in Mn_2SiO_4 with an increase of the fayalite component (Fig. 9a); this trend resembles that of olivines from other alkaline plutonic complexes (e.g. Greenwood and Edgar, 1984; Neumann, 1976).

Pyroxenes. Thirteen pyroxene analyses from the monzodiorite and megaporphyry, together with their corresponding structural formulae are given in Table 5. The average compositions of the monzodiorite and the megaporphyry pyroxenes are $Wo_{46.3}En_{39.3}Fs_{14.4}$ and $Wo_{42.5}En_{38.6}Fs_{18.6}$, respectively. These are that compositions of titanoan-diopside and titanoan-augite according to the nomenclature of Morimoto (1988).

Table 3. Chemical composition of titanomagnetites from the monzodiorite

	7/JB7	15/JB7		7/JB7	15/JB7
TiO_2	11.28	12.50	Ti^{4+}	0.32	0.36
Al_2O_3	1.77	2.01	Al^{3+}	0.08	0.09
Cr_2O_3	0.12	0.21	Cr^{3+}	0.00	0.01
Fe_2O_3	44.77	41.40	Fe^{3+}	1.28	1.19
FeO	40.37	41.05	Fe^{2+}	1.28	1.31
MnO	0.50	1.27	Mn^{2+}	0.02	0.04
MgO	0.49	0.17	Mg^{2+}	0.03	0.01
Total	99.30	98.61	Total	3.00	3.00
End members			Usp.	33.68	37.67
			Mt.	66.33	62.33

Usp. = ulvospinel; Mt. = magnetite, structural formulae on the basis of four oxygens.

Table 4. Chemical composition of olivines of the monzodiorite

	3/JB7	14/JB7	19/JB7	20/JB7	21/JB7	22/JB7	29/JB7
SiO_2	33.96	35.15	35.03	34.96	35.48	35.32	35.54
TiO_2	0.03	0.02	0.04	0.02	0.04	0.02	0.02
FeO	38.80	39.10	38.16	38.17	37.39	37.58	37.98
Cr_2O_3	–	–	–	–	0.06	0.03	–
MnO	1.00	1.15	0.93	1.07	0.92	0.94	1.11
MgO	26.13	25.26	26.55	26.60	26.55	26.40	25.83
Total	99.92	100.68	100.71	100.82	100.44	100.29	100.48
Structural formulae on the basis of four oxygens							
Si^{4+}	0.97	0.99	0.98	0.98	1.00	0.99	1.00
Fe^{2+}	0.93	0.92	0.90	0.90	0.88	0.88	0.89
Mn^{2+}	0.02	0.03	0.02	0.03	0.02	0.02	0.03
Mg^{2+}	1.11	1.06	1.11	1.11	1.11	1.11	1.08
Total	3.03	3.01	3.02	3.02	3.00	3.01	3.00
Fe_2SiO_4	44.91	45.84	44.15	44.04	43.65	43.91	44.60
Mg_2SiO_4	53.92	52.79	54.76	54.71	55.26	54.98	54.08
Mn_2SiO_4	1.17	1.37	1.09	1.25	1.09	1.11	1.3

Table 5. Chemical composition of pyroxenes from both rock types

	Megaporphyry							Monzodiorite					
	1/F3	2/F3	3/F3	4/F3	5/F3	6/F3	7/F3	1/JB7	9/JB7	10/JB7	17/JB7	30/JB7	31/JB7
SiO_2	49.89	49.70	49.03	47.63	49.26	47.58	49.04	50.06	50.07	49.98	48.60	51.08	51.42
TiO_2	1.61	1.42	1.55	1.85	1.84	1.56	1.52	1.01	0.65	0.53	1.14	1.19	1.12
Al_2O_3	2.83	2.47	2.51	3.21	2.99	2.99	2.56	2.63	2.28	2.12	3.09	2.83	2.59
Cr_2O_3	0.03	–	–	0.02	0.01	0.03	–	0.06	0.01	–	0.03	0.02	–
FeO	10.70	13.06	11.76	10.90	10.59	11.32	11.03	8.99	8.97	8.95	8.77	8.55	8.38
MnO	0.26	0.36	0.25	0.22	0.17	0.28	0.23	0.31	0.29	0.29	0.35	0.36	0.29
MgO	13.34	12.24	13.05	13.34	13.44	13.65	13.37	13.30	13.47	13.40	13.39	13.39	13.49
CaO	20.58	19.52	20.33	20.63	20.39	19.75	20.47	21.73	22.14	21.97	21.67	22.16	22.06
Na_2O	0.39	0.41	0.36	0.42	0.35	0.40	0.37	0.77	0.66	0.72	0.84	0.78	0.76
Total	99.65	99.21	98.84	98.22	99.05	97.56	98.61	98.87	98.56	97.96	97.88	100.36	100.11
Structural formulae on the basis of six oxygens													
Si(IV)	1.89	1.90	1.88	1.84	1.87	1.85	1.88	1.90	1.91	1.92	1.87	1.90	1.92
Al(IV)	0.11	0.10	0.11	0.15	0.13	0.14	0.12	0.10	0.09	0.08	0.13	0.10	0.08
T site	2.00	2.00	1.99	1.98	2.00	1.99	2.00	2.00	2.00	2.00	2.00	2.00	2.00
Al(IV)	0.01	0.01	–	–	0.01	–	–	0.02	0.01	0.01	0.01	0.03	0.03
Ti	0.05	0.04	0.04	0.05	0.05	0.05	0.04	0.03	0.02	0.02	0.03	0.03	0.03
Fe^{2+}	0.34	0.42	0.38	0.35	0.34	0.37	0.35	0.29	0.29	0.29	0.28	0.27	0.26
Mn^{2+}	0.01	0.01	0.01	0.01	0.01	0.01	0.01	0.01	0.01	0.01	0.01	0.01	0.01
Mg	0.75	0.70	0.75	0.77	0.76	0.79	0.76	0.75	0.77	0.77	0.77	0.74	0.75
Ca	0.83	0.80	0.84	0.85	0.83	0.82	0.84	0.88	0.90	0.90	0.89	0.89	0.88
Na	0.03	0.03	0.03	0.03	0.03	0.03	0.03	0.06	0.05	0.05	0.06	0.06	0.05
M1, M2	2.02	2.02	2.04	2.07	2.02	2.07	2.04	2.04	2.05	2.05	2.06	2.03	2.02
Q	1.92	1.92	1.96	1.97	1.93	1.98	1.96	1.92	1.96	1.96	1.94	1.90	1.89
FS	17.51	21.67	19.18	17.77	17.41	18.48	17.99	14.85	14.62	14.68	14.52	14.06	13.81
EN	38.91	36.22	37.94	38.77	39.38	39.73	38.87	39.16	39.14	39.17	39.52	39.25	39.62
WO	43.15	41.51	42.47	43.10	42.93	41.32	42.77	45.99	46.24	46.15	45.96	46.69	46.57
X Fe	0.31	0.37	0.34	0.31	0.31	0.32	0.32	0.27	0.27	0.27	0.27	0.26	0.26
X Ca	0.43	0.42	0.43	0.43	0.43	0.42	0.43	0.46	0.46	0.46	0.46	0.47	0.47
T (°C)	903	935	919	902	918	1004	892	741	741	741	741	664	664

$Q = Ca + Fe^{2+} + Mg$; $X\,Fe = Fe^{2+}/Fe^{2+} + Mg$; $X\,Ca = Ca/Ca + Mg + Fe^{2+}$. T(°C) = calculated temperature from Kretz calibration.

On the $SiO_2 - Al_2O_3$ plot (Le Bas, 1962) the pyroxenes of the megaporphyry plot in the alkaline field whereas those of the monzodiorite straddle both alkaline and subalkaline fields (Fig. 9 b). A positive linear relationship between Ti and Al(IV) is obvious for the megaporphyry (Fig. 9 c). Such a relationship was reported for pyroxenes from other alkaline complexes (Scott, 1980; Greenwood and Edgar, 1984; Almond, 1988). The MgO/FeO ratios of

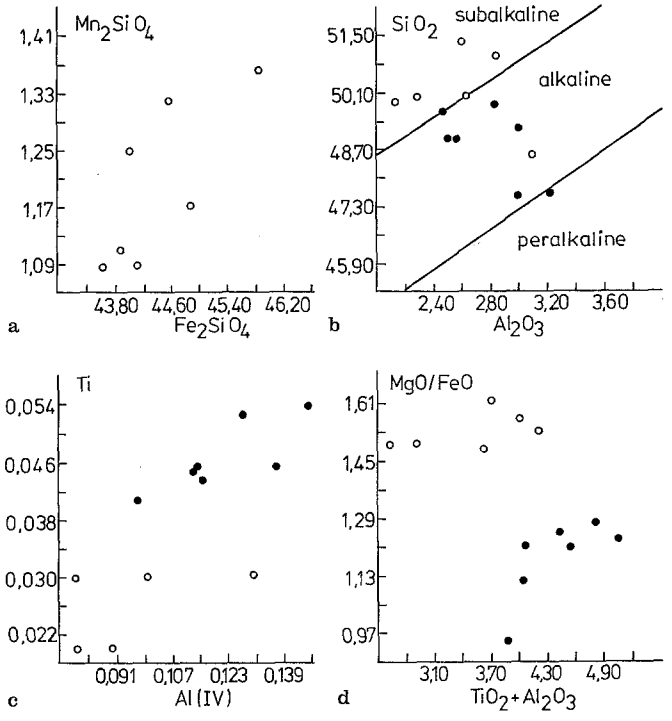

Fig. 9 *a–d.* Chemical variation diagrams of olivines and pyroxenes. a Mn_2SiO_4 versus Fe_2SiO_4 (mol.%) of the olivines. b SiO_2 versus Al_2O_3 (wt.%) of the pyroxenes. The dividing lines are after Le Bas (1962). c Ti versus Al(IV) at. of the pyroxenes. d (MgO/FeO) versus $TiO_2 + Al_2O_3$ wt.% of the pyroxenes. Symbols: open circles = pyroxenes and olivines from monzodiorite; closed circles = pyroxenes and olivines from megaporphyry

the pyroxenes are plotted against $(TiO_2 + Al_2O_3)$ in Fig. 9d. The pyroxenes of the megaporphyry display lower MgO/FeO ratios and higher $TiO_2 + Al_2O_3$ contents, which is in accordance with the bulk chemistry of the host rocks.

The transfer equilibrium reaction thermometer of Kretz (1982) and the graphic pyroxene thermometer of Lindsley (1983) are applied to estimate the crystallization temperatures of both rock varieties. The Kretz calibration has the form $T = 1000/(0.054 + 0.608X^{Cpx} - 0.304\ln(1-2[Ca])$, where T is the absolute temperature, X is $Fe^{2+}/(Mg + Fe^{2+})$ and [Ca] is $Ca/(Ca + Mg + Fe^{2+})$ in Cpx.

Fig. 10. Pyroxene compositions (mol.%) plotted on the pyroxene quadrilateral. The isotherms at 1 atm (Lindsley, 1983) are also projected. Temperatures are in °C. Symbols: open circles = pyroxenes from monzodiorite; closed circles = pyroxenes from megaporphyry

The calculation of temperature by this calibration is based on the data listed in Table 5. Average temperatures for the megaporphyry and the monzodiorite are 924 and 715 °C, respectively. On the other hand, Lindsley's thermometer gave corresponding temperatures of 800 and 600 °C at 1 kbar. (Fig. 10). However, these estimates are minimum temperatures due to the presence of a single pyroxene. The occurrence of diopside–hypersthene–hornblende–biotite hornfels in the Saramuj sediments adjacent to the contact of the monzodiorite favours the temperature estimates after Kretz as more reliable.

Feldspars. The chemical data and structural formulae of 12 feldspar grains are listed in Table 6 and are plotted on the Ab–An–Or ternary diagram (Fig. 11). The monzodiorite contains plagioclase with the average composition of An_{49} whereas the mean composition of two megacrysts from the megaporphyry is An_{56} (average of 29 point analyses). The significant anorthite difference between the megacrysts and the groundmass lathy plagioclases (An_{1-39}) implies that the megacrysts were not in equilibrium with the host melts at the time of emplacement.

The bulk analyses of the megacrysts show a lower An content and higher orthoclase (up to 17 mol.%) content than the microprobe point analyses. The high proportion of orthoclase can only be understood if the highly sericitized nature of some megacrysts is taken into account, because the solubility of the orthoclase component in plagioclase does not exceed 4–5% even at high water pressures (Smith and Brown, 1988). The alkali feldspars of the monzodiorite are albite-rich and contain up to 6 mol.% anorthite. These are mesoperthites according to Smith and Brown (1988). The megacrysts are unzoned on the scale of the thin section. However, our analyses do not rule out the possibility of large-scale zoning taking into consideration the large size of these phenocrysts.

Biotite. The analyses of five biotite grains and their structural formulae are listed in Table 7. They have the following average chemical formula: $(K_{1.78}Na_{0.15})(Mg_{3.13}Fe_{1.82}Ti_{0.64})(Si_{5.42}A_{12.4}Ti_{0.17})\ O_{22}$ which corresponds to a phlogopitic biotite (Deer et al., 1962). Titanium oxide is extremely high (up to 7.76 wt.%). It is

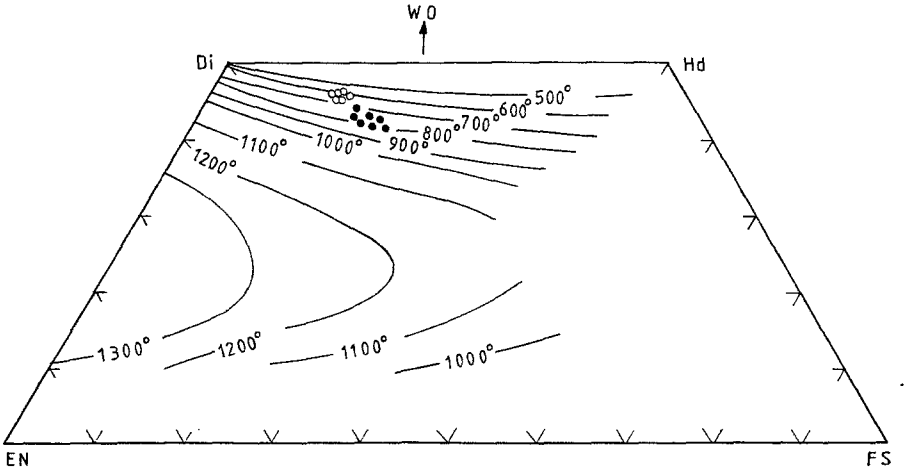

Table 6. Feldspar chemical data

	Monzodiorite					Megaporphyry						
	8/JB7	24/JB7	26/JB7	27/JB7	28/JB7	FS.GJ	C44/FS	44/FS1	F1	F2	F3/1	F3/2
SiO_2	64.96	55.78	56.35	65.19	64.57	57.20	58.85	61.79	54.43	54.67	66.92	59.17
TiO_2	0.14	0.06	0.11	0.18	0.14	–	–	–	–	–	–	–
Al_2O_3	19.60	27.28	27.15	19.80	19.85	26.65	25.89	24.95	28.14	28.31	20.58	21.51
FeO	0.11	0.19	0.13	0.11	0.08	0.45	0.93	0.57	0.53	0.58	0.19	2.93
CaO	1.06	9.89	9.89	1.21	1.21	9.10	5.88	5.32	11.21	10.81	0.58	4.57
Na_2O	4.59	5.54	5.63	4.56	4.66	5.25	4.64	4.75	4.49	4.41	9.93	5.40
K_2O	9.39	0.37	0.31	8.78	8.62	0.45	2.39	2.51	0.44	0.48	0.47	3.71
MnO	0.01	–	0.01	0.01	0.08	–	–	–	–	–	–	–
Total	99.86	99.11	99.58	99.84	99.21	99.10	98.58	99.89	99.24	99.26	98.67	97.29
Structural formulae on the basis of eight oxygens												
Si^{4+}	2.95	2.53	2.54	2.95	2.94	2.59	2.67	2.75	2.48	2.48	2.96	2.76
Al^{3+}	1.05	1.46	1.44	1.05	1.06	1.42	1.38	1.31	1.51	1.52	1.07	1.18
Fe^{2+}	0.00	0.01	0.00	0.00	0.00	0.02	0.04	0.02	0.02	0.02	0.01	0.11
Ca^{2+}	0.05	0.48	0.48	0.06	0.06	0.44	0.29	0.25	0.55	0.53	0.03	0.23
Na^{1+}	0.40	0.49	0.49	0.40	0.41	0.46	0.41	0.41	0.40	0.39	0.85	0.49
K^{1+}	0.54	0.02	0.02	0.51	0.50	0.03	0.14	0.14	0.03	0.03	0.03	0.22
Total	5.00	4.99	4.99	4.97	4.98	4.95	4.92	4.88	4.98	4.97	4.94	5.00
OR	54.42	2.16	1.81	52.49	51.56	2.80	16.62	17.68	2.64	2.95	2.93	23.55
AB	40.43	49.25	49.83	41.43	42.36	49.65	49.04	50.85	40.91	41.22	94.04	52.09
AN	5.16	48.59	48.37	6.08	6.08	47.55	34.34	31.47	56.45	55.83	3.04	24.36

F1 and F2 are microprobe analyses of megacrysts; F3/1 and F3/2 are groundmass plagioclases; the samples FS.GJ, C44/FS and 44/FS1 are ICP bulk analyses of megacrysts.

Table 7. Chemical analyses and structural formulae of biotites from the monzodiorite

	6/JB7	12/JB7	13/JB7	16/JB7	18/JB7
SiO_2	35.88	37.63	36.90	35.52	37.32
TiO_2	7.54	7.23	7.38	7.76	6.69
Al_2O_3	13.71	13.63	13.95	13.65	13.93
FeO	14.79	15.05	14.74	14.23	14.56
MgO	14.52	13.92	14.04	14.09	14.25
MnO	0.06	0.06	0.15	0.13	0.10
Na_2O	0.41	0.49	0.48	0.48	0.74
K_2O	9.63	9.39	9.55	9.42	9.20
Total	96.54	97.40	97.19	95.28	96.79
Structural formulae based on 22 oxygens					
Si^{4+}	5.34	5.52	5.43	5.34	5.49
Al^{3+}	2.40	2.35	2.42	2.42	2.42
Ti(IV)	0.26	0.13	0.15	0.24	0.09
T site	8.00	8.00	8.00	8.00	8.00
Ti(IV)	0.58	0.67	0.67	0.64	0.65
Fe^{2+}	1.84	1.84	1.81	1.79	1.79
Mg	3.22	3.04	3.08	3.16	3.13
Mn^{2+}	0.01	0.01	0.02	0.02	0.01
O site	5.65	5.56	5.58	5.60	5.59
Na	0.12	0.14	0.14	0.14	0.21
K	1.83	1.76	1.79	1.81	1.73
A site	1.95	1.90	1.93	1.95	1.94
Total	15.59	15.46	15.51	15.55	15.53

present mainly in the octahedral sites and roughly 25% of the Ti is present in the tetrahedral sites substituting for silicon. Serdyuchenko (1948) suggested that at high temperatures and under alkaline conditions the partially filled tetrahedral sites are completed by titanium.

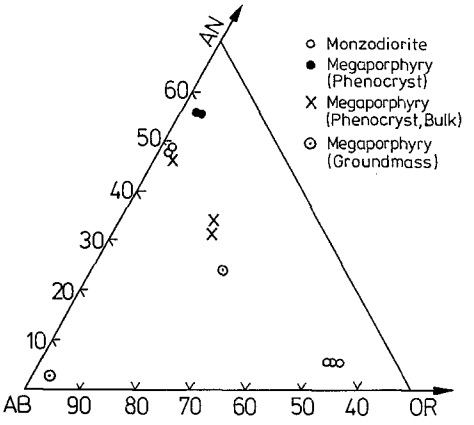

Fig. 11. Feldspar compositions (mol.%) plotted on the An–Ab–Or ternary

Discussion

Petrographic and geochemical data place constraints on the pressure/temperature conditions of the magmatic evolution. The presence of diopside, hypersthene and relics of hornblende, together with widespread biotite and anorthite-rich plagioclase in the innermost aureole of the contact metamorphosed Saramuj Conglomerate, characterizes a lower granulite facies metamorphism (e.g. Miyashiro, 1979). Consequently, the temperature in the innermost aureole must have exceeded 600 °C. This is in favour of regarding 715 °C (Kretz calibration) as the crystallization temperature of the monzodiorite rather

than 600 °C (Lindsley thermometer). The corresponding temperature of the megaporphyry is about 924 °C.

The depth of the intrusion of the monzodiorite can be placed at about 3 – 4 km according to the mineral paragenesis of the epimetamorphic Saramuj Conglomerate. Field evidence, age relationships and chemical variation diagrams suggest a possible cogenetic origin for the monzodiorite and the megaporphyry. The relatively higher contents of the LILE in the monzodiorite compared with the megaporphyry is interpreted in terms of crustal assimilation. However, in case of crustal assimilation a relatively elevated initial Sr ratio of the monzodiorite is expected. It must be borne in mind that the presumably assimilated crustal rocks have characteristically low initial Sr ratios and are not essentially older than the monzodiorite. The Pan-African granitoids of south-west Jordan were emplaced between 625 and 600 Ma and have an average Sr_i of 0.703 4 (Jarrar, 1985; Brook et al., 1990). Consequently, the low Sr_i ratio of the monzodiorite (0.703 6) does not contradict the assumption of possible crustal contamination.

The bulk and mineral chemistry (Figs. 6, 7 and 9) of the monzodiorite and megaporphyry are typical of alkaline rocks and correlative with rift-related alkaline complexes.

The Mg # of both rock varieties is <0.55. Wilkinson (1982) demonstrated that even the iron-rich mantle with Mg # = 0.80 would be in equilibrium with melts having Mg # = 0.57. Ringwood (1975) and Green (1980) showed that a magma produced by partial melting of a normal lherzolitic mantle source would contain 300 – 400 ppm Ni and 400 – 500 ppm Cr. The low abundances of compatible elements of the megaporphyry and the monzodiorite and the low Mg # are arguments in favour of derivative magmas for both rock types. The low contents of Cr and Ni are explained by fractionation of forsteritic olivine and clinopyroxene (Green, 1980).

The LILE enrichments in both rock types in general and in the monzodiorite in particular can be attributed to fractional crystallization and the assimilation of crustal material. The latter applies for the monzodiorite and is supported by the occurrence of syenite xenoliths. The trough at Nb (Fig. 7) also suggests this conclusion, although the Nb anomaly can be alternatively interpreted in terms of mantle metasomatism (Fitton et al., 1988).

Owing to the intrusive nature and in accordance with the age of emplacement of the monzodiorite the Saramuj Conglomerate cannot be younger than 595 Ma. The Saramuj Conglomerate in turn discordantly overlies a 610 ± 5 Ma older granodiorite in Wadi Abu Barqa (Jarrar, 1985). The components of the Saramuj Conglomerate were exclusively derived from this granodiorite, other monzogranites and volcanic clasts of bimodal composition. On the other hand, metamorphic clasts are subordinate (about 1%). The monzogranites were emplaced at about 600 Ma (Brook et al., 1990). Unfortunately, no age data are available for the bimodal dykes. However, their age can be constrained from their mode of occurrence, i.e. they intrude the granitoids (610 – 600 Ma) and are present as clasts in the conglomerate. No single bimodal dyke was reported to intrude the Saramuj Conglomerate. Consequently, their emplacement should be at about 600 Ma. On the basis of this discussion the Saramuj Conglomerate cannot be much older than 600 Ma.

The bimodal dyke activity in southern Jordan coincides with a reported transition in the tectonic style from compressional to extensional in the north-eastern desert of Egypt at about 600 Ma (Stern and Hedge, 1985). Furthermore, Stern and Voegeli (1987) and Stern and Manton (1987) reported ages of around 590 Ma for bimodal dyke swarms from the north-eastern desert of Egypt and southern Sinai. This implies that the bimodal activity began in southern Jordan about 10 Ma earlier than in the north-eastern desert and Sinai. However, this needs confirmation by isotopic dating of the bimodal activity in southern Jordan.

Regional implications of the magmatic activity

The Pan-African evolution of the late Proterozoic basement in Jordan was dominated by voluminous calc-alkaline granitoids (625 – 600 Ma; Jarrar, 1985). The transition from an orogenic to an anorogenic regime is marked by an intra-Proterozoic unconformity (Fig. 12). Diagnostic for the anorogenic evolution is a rift-related molasse sedimentation (Saramuj Conglomerate) and a bimodal volcanism of an alkaline to peralkaline character (Jarrar et al., 1992), which is well documented in other parts of the Arabian – Nubian Shield (e.g. Bentor, 1985). The anorogenic magmatism began in Jordan with the emplacement of bimodal dyke swarms, which are represented in the Saramuj Conglomerate by angular pebbles. The monzodiorite intruded the Saramuj at about 595 Ma. Therefore, the Saramuj Conglomerate in its type locality cannot be younger than about 595 Ma.

The late Precambrian crustal evolution of south-west Jordan was equivalent to that of the north-eastern desert of Egypt, which has been evaluated by Willis et al. (1988). These workers described a late Precambrian crustal evolution that concluded in a major episode of crustal extension accompanied by bimodal igneous activity and the deposition of clastic sediments in restricted terrigenous basins. The Saramuj Conglomerate is, on the basis of its age, comparable with the lower half of the Hammamat series of Egypt. Nevertheless, the former is of a conglomeratic nature whereas the latter is composed of a massive polymictic breccia.

According to Bentor (1961; 1985) the Elat conglomerate interfingers with the Katharina province volcanics and they together form the Volcano-Conglomeratic Complex. Bentor suggested that this complex is equivalent to the Saramuj Conglomerate. However, we prefer to correlate this complex with the Saramuj Conglomerate and the overlying Hiayala Volcanoclastic Formation and the Aheimir volcanic suite.

The Shammar Group is widespread in the northern part of the Arabian Shield and it has a thickness between

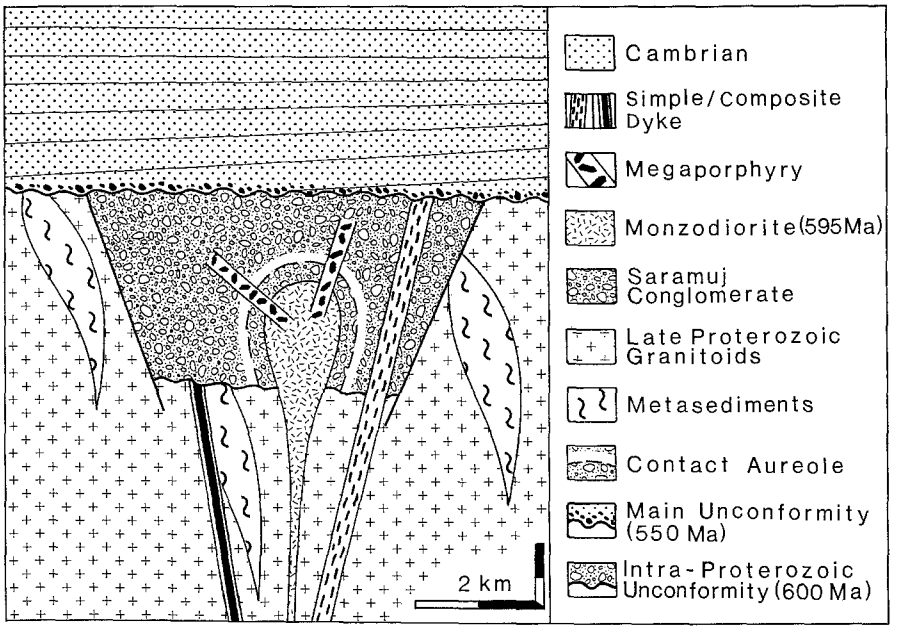

Fig. 12. Schematic cross-section of the Pan-African basement and the rift related molasse basin in south-west Jordan

		SAUDI ARABIA	NE DESERT, EGYPT	SINAI-NEGEV	SW JORDAN
CAMBRIAN	PLATFORM	NUBIAN SANDSTONE			
	530 ± 10Ma				
LATE PROTEROZOIC	PAN AFRICAN MOLASSE	JUBAYLAH Group (540-520 Ma) SHAMMAR Group volcanics interbedded with coarse continental clastics (alluvial to lacustrine) and intruded by alkali granites at 600±24 Ma	"post Hammamat felsites" DOKHAN volcanics (592±26 Ma) partially coeval with the HAMMAMAT Formation (600-590 Ma) sandstones, siltstones, shales and massive polymictic breccia	KATHARINA PROVINCE (580-550 Ma) volcanics interfinger with ELAT Conglomerate and form the "volcano-conglomeratic complex"	AHEIMIR & FEINAN volcanics (~550 Ma) HIAYALA volcani-clastic Formation SARAMUJ Conglo-merate (>595 Ma)
	600 Ma	REGIONAL UNCONFORMITY			
	PAN AFRICAN BASEMENT	monzogranitic plutonism (640-610 Ma)	mesozonal granodiorites (670-610 Ma)	UMM - MALAQ biotite granite (597±22 Ma)	ABU BARQA grano-diorite (610±5 Ma)

Fig. 13. Stratigraphic position of the Saramuj Conglomerate in relation to other Pan-African molasse occurrences of the Arabian–Nubian Shield. The data are compiled from Bielski (1982), Bentor (1961; 1985), Delfour (1970), Greenwood et al. (1976), Jarrar (1985), McCourt (1988), Odin et al. (1983), Stoeser and Camp (1985), Willis et al. (1988), Baubron et al. (1976) and Hadley and Schmidt (1980)

1000 and 14000 m (Hadley and Schmidt, 1980). The Shammar rocks consist of alkaline volcanics and about 15% interbedded coarse continental clastics, which indicate an alluvial to lacustrine environment of deposition. The youngest rhyolite in the Shammar Group is 555 ± 25 Ma (Baubron et al., 1976). The Shammar Group was further intruded by two alkali granites at about 600 ± 24 and 571 ± 8 Ma ago (Baubron et al., 1976).

Figure 13 summarizes the stratigraphic relationships between the Saramuj Conglomerate and its probable time equivalent sequences in the Arabian–Nubian Shield. The orogenic Pan-African basement is transgressively

overlain by molasse sequences, which consist of polymictic conglomerates of exclusively crystalline composition, which are in turn overlain and/or intruded by volcaniclastics of an alkaline to peralkaline nature.

Conclusions

1. The alkaline intrusion of Wadi Qunaia consists of a monzodiorite and a megaporphyry, both intruding the late Proterozoic Saramuj Conglomerate.
2. The chondrite normalized trace element diagram (Fig. 7) is correlative with continental rift zone magmatism.
3. The field, petrographic and geochemical criteria are in favour of a consanguineous relationship between the two magmatic bodies.
4. The formation of the unzoned labradorite megacrysts of the megaporphyry indicates a long-term steadiness of the pressure – temperature conditions in the magma chamber.
5. The low Mg #, lower Mg/Fe ratios of the pyroxenes, and absence of olivine in the megaporphyry support the derivation of the megaporphyry from the monzodiorite.
6. The irregular arrangement of the megacrysts in the groundmass supports a turbulent ascent triggered by a sudden pressure release.
7. The age of the Saramuj Conglomerate in its type locality is constrained between 600 and 595 Ma. Furthermore, the Saramuj Conglomerate is equivalent to the lower part of the Hammamat series, north-eastern desert of Egypt, the polymictic conglomerate of the Shammar group, northern Saudi Arabia and the Elat conglomerate, north-east Sinai.

Acknowledgements We are indebted to Dr Ackermand, Mineralogical Institute, Kiel University for operating the microprobe analyses. The isotopic dating was carried out at the Zentrallaboratorium für Geochronologie (ZLG, Director Professor Dr B. Grauert), Münster University. Two authors (W & Z) also gratefully acknowledge accommodation and facilities provided by the University of Jordan, Amman. The research was supported by the German Science Foundation (DFG) under the contract Wa 26/15-1. The manuscript has been improved by constructive comments of Dr R. Stern, University of Texas at Dallas, USA, and two anonymous reviewers. Ina Schmelzer is strongly acknowledged for improving the manuscript.

References

Almond DC (1988) Chemical fractionation in titaniferous clinopyroxene from Bayuda, Sudan. Can Mineral 26: 1027–1035

Baubron JC, Delfour J, Vialette Y (1976) Geochronologic measurements (Rb/Sr; K/Ar) on rocks of the Arabian Shield, Kingdom of Saudi Arabia. Saudi Arabian Dir. Gen. Min. Res. Tech. Rep. 76-JED-22: 152 pp.

Bender F (1974) Explanatory notes on the geological map of Wadi Araba, Jordan (scale 1 : 100 000, 3 sheets). Geol. Jahrb. 10: 3–62

Bentor YK (1961) Petrographical outline of the Precambrian in Israel. Bull Res Coun Israel, Sect G 10G: 19–63

Bentor YK (1985) The crustal evolution of the Arabo-Nubian massif with special reference to Sinai Peninsula. Precambrian Res 28: 1–74

Bielski M (1982) Stages in the evolution of the Arabian–Nubian Massif in Sinai. Ph D Thesis, Hebrew University, Jerusalem: 155 pp.

Blanckenhorn M (1912) Naturwissenschaftliche Studien am Toten Meer und im Jordantal. Friedlaender, Berlin

Blaxland A, Gohn E, Haack U, Hoffer E (1979) Rb-Sr ages of late tectonic granites in the Damara orogen, SW Africa, Namibia. N Jb Miner Mh 11: 498–508

Brook M, Ibrahim K, McCourt WJ (1990) New geochronological data from the Arabian shield area of SW Jordan. Proceedings of the 3rd Jordan Geological Conference: 361–394

Carmichael ISE (1967) The iron-titanium oxides of salic volcanic rocks and their associated ferromagnesian silicates. Contrib Mineral Petrol 14: 36–64

Cooper JA, Stacey JS, Fleck RJ (1979) An evaluation of the zircon method of isotope dating in the southern Arabian Shield. Contrib Mineral Petrol 68: 429–439

Cox KG, Bell JD, Pankhurst RJ (1979) The Interpretation of Igneous Rocks. Allen & Unwin, London: 450 pp.

Deer WA, Howie RA, Zussman J (1962) Rock-forming Minerals (Sheet Silicates). Longman, London

De La Roche H, Leterrier P, Grandclaude P, Marchal M (1980) A classification of volcanic and plutonic rocks using R1-R2 diagram and major element analyses. Its relationship with current nomenclature. Chem Geol 29: 183–210

Delfour J (1970) Le groupe de J'Balah. BRGM Bull Ser 2, Sec IV 4: 19–32

Fitton JG, James D, Kempton PD, Ormerod DS, Leeman WP (1988) The role of lithospheric mantle in the generation of late Cenozoic basic magmas in the western United States. J Petrol Spec Lithosphere Issue: 331–349

Frey M, De Capitani C, Liou JG (1991) A new petrogenetic grid for the low-grade metabasite. J Metamorphic Geol 9: 497–509

Friz-Töpfer A (1991) Geochemical characterization of Pan-African dyke swarms in southern Sinai: from continental margin to intraplate magmatism. Precambrian Res 49: 281–300

Green TH (1980) Island arc and continent building magmatism – a review of petrogenetic models based on experimental petrology and geochemistry. Tectonophysics 63: 367–385

Greenwood RC, Edgar AD (1984) Petrogenesis of gabbros from Mt. St. Hilaire, Quebec, Canada. Geol J 19: 353–376

Greenwood WR, Hadley DG, Anderson RE, Fleck RJ, Schmidt DL (1976) Late Proterozoic cratonization in southwestern Saudi Arabia. Phil Trans R Soc London Ser A 280: 517–527

Hadley DG, Schmidt DL (1980) Sedimentary rocks and basins of the Arabian Shield and their evolution. In: Cooray P G, Tahoun S A, eds. Evolution and mineralization of the Arabian–Nubian Shield. Inst Appl Geol Jeddah Bull 3, 4: 25–50

Irvine TN, Baragar WRA (1971) A guide to the chemical classification of the common volcanic rocks. Cana J Earth Sci 8: 523–548

Jarrar G (1985) Late Proterozoic crustal evolution of the Arabian–Nubian Shield in Wadi Araba area, SW Jordan. Geol Jahrb 61: 3–87

Jarrar G, Wachendorf H, Zellmer H (1991) The Saramuj Conglomerate: Evolution of a Pan-African molasse sequence from southwest Jordan. N Jahrb Geol Paläont Mh H 6: 335–356

Jarrar G, Wachendorf H, Saffarini G (1992) A late Proterozoic bimodal volcanic/subvolcanic suite from Wadi Araba, SW Jordan. Precambrian Res 56: 51–72

Kretz R (1982) Transfer and exchange equilibria in a portion of the pyroxene quadrilateral as deduced from natural and experimental data. Geochim Cosmochim Acta 46: 411–421

Krogh TE (1973) A low contamination method for hydrothermal decomposition of zircons and extraction of U and Pb for isotopic age determination. Geochim Cosmochim Acta 37: 485–494

Le Bas MJ (1962) The role of aluminium in igneous pyroxenes with relation to their parentage. Am J Sci 260: 267–288

Lenz H, Bender F, Besang C, Harre W, Kreuzer H, Müller P, Wendt I (1972) The age of early tectonic events in the zone of the Jordan Geosuture based on radiometric data. 24th International Geological Congress Section 3: 371–379

Lindsley DH (1983) Pyroxene thermometry. Am Mineral 68: 477–493

Ludwig KR (1980) Calculation of uncertainties of U-Pb isotope data. Earth Planet Sci Lett 46: 212–220

McCourt WJ (1988) The geology, geochemistry and tectonic setting of the granitic rocks of SW Jordan. Bull NRA, Geol Div Amman: 10

Miyashiro A (1978) Nature of alkalic volcanic rock series. Contrib Mineral Petrol 66: 91–104

Miyashiro A (1979) Metamorphism amd Metamorphic Belts. Allen & Unwin, London: 492 pp.

Morimoto N (1988) Nomenclature of pyroxenes. Report of the Subcommittee on Pyroxenes, IMA. Min Mag 52: 535–550

Neumann ER (1976) Compositional relations using pyroxenes, amphiboles and other mafic phases in the Oslo region plutonic rocks. Lithos 9: 85–109

Odin GS, Gale NH, Auvray B, Bielski M, Doré F, Lancelot JR, Pasteels P (1983) Numerical dating of Precambrian-Cambrian boundary. Nature 301: 21–23

Pallister JS, Stacey JS, Fischer LB, Wayne RP (1988) Precambrian ophiolites of Arabia: geologic settings, U-Pb geochronology, Pb-isotope characteristics, and implications for continental accretion. Precambrian Res 38: 1–54

Phinney WC, Morrison DA, Maczuca DE (1988) Anorthosites and related megacrystic units in the evolution of Archean crust. J Petrol 29: 1283–1323

Reymer APS, Mathews A, Navon O (1984) Pressure-temperature conditions in the Wadi Kid metamorphic complex: implications for the Pan-African event in SE Sinai. Contrib Mineral Petrol 85: 336–345

Ringwood AE (1975) Composition and Petrology of the Earth's Mantle. McGraw-Hill, New York

Scott PW (1976) Crystallization trends of pyroxenes from the alkaline volcanic rocks of Tenerife, Canary Islands. Min Mag 40: 805–816

Serdyuchenko DP (1948) On the crystallochemical role of titanium in micas. Dokl Akad Sci USSR 59: 739

Smith JV, Brown WL (1988) Feldspar Minerals: Crystal Structures, Physical, Chemical, and Microtextural Properties. Vol 1, 2nd edn. Springer Verlag, Berlin: 828 pp.

Stacey JS, Kramers JD (1975) Approximation of terrestrial lead isotope evolution by a two-stage model. Earth Planet Sci Lett 26: 207–221

Steiger RH, Jäger E (1977) Subcommission on Geochronology: convention on use of decay constants in geo- and cosmochronology. Earth Planet Sci Lett 36: 359–362

Stern RJ, Hedge CE (1985) Geochronologic and isotopic constraints on late Precambrian crustal evolution in the Eastern Desert of Egypt. Am J Sci 285: 97–127

Stern RJ, Manton WI (1987) Age of Feiran basement rocks, Sinai: implications for late Precambrian crustal evolution in the northern Arabian–Nubian Shield. J Geol Soc London 144: 569–575

Stern RJ, Voegeli DA (1987) Geochemistry, geochronology, and petrogenesis of a Late Precambrian (= 590 Ma) composite dike from the North Eastern Desert of Egypt. Geol Rundsch 76: 325–341

Stern RJ, Gottfried D, Hedge CE (1984) Late Precambrian rifting and crustal evolution in the northeastern desert of Egypt. Geology 12: 168–172

Stoeser DB, Camp VE (1985) Pan-African microplate accretion of the Arabian Shield. Bull Geol Soc Am 96: 817–826

Streckeisen A (1976) To each plutonic rock its proper name. Earth Sci Rev 12: 1–33

Thompson RN, Morrison MA, Hendry GL, Parry SJ (1984) An assessment of the relative roles of a crust and mantle in the magma genesis: an elemental approach. Phil Trans R Soc London A310: 549–590

Wilkinson JFG (1982) The genesis of mid-ocean ridge basalt. Earth Sci Rev 18: 1–57

Willis KM, Stern RJ, Clauer N (1988) Age and geochemistry of late Precambrian sediments of the Hammamat series from the Northeastern Desert of Egypt. Precambrian Res 42: 173–187

Wilson M (1989) Igneous Petrogenesis: A Global Tectonic Approach. Allen & Unwin, London: 466 pp.

York D (1969) Least squares fitting of a straight line with correlated errors. Earth Planet Sci Lett 5: 320–324